VECIMS 2008 – IEEE International Conference on
Virtual Environments, Human-Computer Interfaces, and Measurement Systems
Istambul, Turkey, 14-16 July 2008

Modeling of Flexible Needle for Haptic Insertion Simulation

Xuejian He, Yonghua Chen and Libo Tang
Department of Mechanical Engineering, The University of Hong Kong
Haking Wong Building, Pokfulam Road, Hong Kong, China
Phone: +852-2859-7910, Fax: +852-2858-5415, Email: *yhchen@hku.hk*

Abstract – *Needle buckling is commonly observed in the surgical procedure of flexible needle insertion. Unexpected buckling can seriously affect the insertion performances, and it should be avoided because it causes unstable and undesirable motion of the needle, thereby damages surrounding vital tissue structures. Although needle insertion simulation methods using haptic interfaces have been reported, yet no extensive study of needle buckle modeling and its haptic simulation can be found. Therefore, in this paper modeling methods of needle buckling in air, buckling in homogeneous tissue, and buckling in multi-layered tissues are proposed. An energy-based method is used to model the feedback force in the insertion procedure through a haptic interface. An experimental simulation system based on a haptic interface is developed.*

Keywords *– flexible needle, haptics, needle insertion, buckling.*

I. INTRODUCTION

Percutaneous insertion of needles is one of the most common procedures encountered in clinical practice. Such procedure usually involves inserting slender needles into soft and inhomogeneous tissue with limited visual feedback, thus it is a task requiring good skill and care. Computer simulation as an intuitive means for training and planning of such procedure has obvious advantages. It has therefore increasingly attracted researchers' attention. However, it is a great challenge to faithfully simulate the surgical procedure since it involves tissue deformation, needle-tissue interaction, needle deflection and tool force modeling. It requires much knowledge on mechanics, medicine, biology, and computer. Though much work has been done, e.g. [5~8], the simulation of flexible needle buckling and deflection during needle insertion is less studied. Needle buckling is commonly observed and can greatly affect the insertion performance, and it can also be utilized to control the insertion path inside tissue. Sometimes, the needle buckling should be avoided because unexpected force change due to buckling will make the needle to deviate from the anticipated path. Such sudden change of motion might result in damage to surrounding vital tissues, such as nerve and artery. Hence, buckling should be taken into account in order to realistically simulate the needle insertion process. Although the modeling methods of soft tissue deformation are widely studied in computer simulation, they are mainly based on homogeneous tissue. However, deformation models of homogeneous tissue are incapable of realistically simulating the inhomogeneous tissue deformation in the needle insertion scenario. Therefore, the main contributions of this paper are as the following:

- Euler theory and numerical solution of buckling are combined to model needle buckling in homogeneous and layered tissue;
- Column-beam theory is used to model large needle deflection after buckling occurs;
- An approach based on fracture mechanics is used to model the feedback force for haptic rendering.

A flexible needle insertion simulator based on haptic modeling is proposed as shown in Fig. 1, in which a user can feel the effect of needle buckling and see the deflection. When buckling occurs, the needle deflects and the feedback force the user feels through a haptic stylus fluctuates suddenly. The virtual environment of the simulation is mainly composed of three parts: tissue deformation modeling, needle buckling and deflection modeling, and haptic rendering. The haptic interface tracks a user's hand movements and reads its pose (positions and orientations). This pose is used by the computer to control the virtual needle. According to the interaction of needle and tissue, the needle deflection and tissue deformation are computed by the computer. At the same time, the force is calculated and sent to the haptic interface. As a result, the user can feel the feedback force.

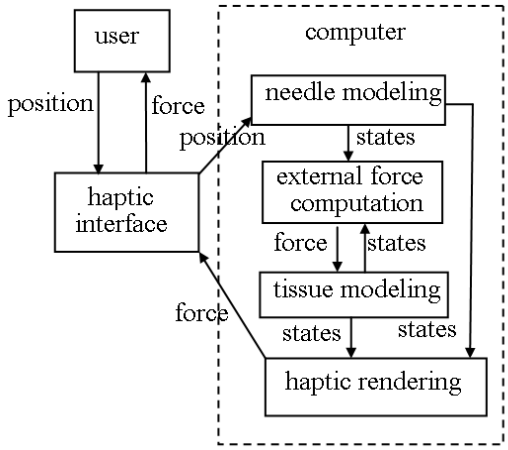

Fig.1. A block diagram showing the haptic simulation of flexible needle insertion.

The rest of the paper is organized as follows. In section II, the modeling of needle buckling and deflection is explained. A haptic rendering method based on fracture mechanics is described in section III, and an experimental simulation system is introduced in section IV. Finally, we summarize the work and discuss the future research directions.

II. FLEXIBLE NEEDLE MODELING

In this section, the models of needle buckling and deflection are proposed. The buckling model in air is explained in section A, and the buckling model in homogeneous tissue is described in section B. A needle buckling model in multi-layered materials is proposed and discussed in section C.

A. Needle Buckling in Air

A long, slender elastic column under an axial load will fail by buckling (Fig. 2). Buckling is a failure mode characterized by a sudden failure of a structural member subjected to high compressive stresses, where the actual compressive stresses at failure are smaller than the ultimate compressive stresses that the material is capable of withstanding. The buckling effect is so large that the effect of the direct load may be neglected.

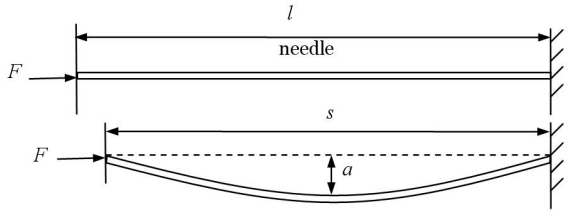

Fig. 2. Schematic of needle buckling.

In 1757, Euler derived a formula governing the maximum axial load that a long, slender, ideal column can carry without buckling. The maximum load, sometimes called the critical load, causes the column to be in a state of unstable equilibrium; that is, any increase in the load, or the introduction of the slightest lateral force, will cause the column to fail by buckling. The Euler formula [2] for columns with one end fixed is:

$$P_e = \frac{\pi^2 EI}{4l^2} \tag{1}$$

where P_e is the maximum or critical force (axial load on column), E is the modulus of elasticity, I is the area moment of inertia, and l is the unsupported length of column. For a needle with a length of 100 *mm*, Young's modulus of 2×10^{11} *pa*, its critical force varying with needle radius is plotted in Fig. 3(a). The curve is plotted based Equation (1), and the points marked in green rectangles are calculated by an FEM software package, COSMOS®/FFE[9], which uses linear buckling mode. It can be seen from the figure that when the needle diameter is larger than 0.8 *mm*, it's buckling critical force increases quickly. Fig. 3(b) shows the relation between needle buckling critical force and its length. In this context, the needle radius is fixed at 0.3 *mm*. When the needle length is larger than 50 *mm*, its critical force decreases very slowly as its length increases. It can be seen from Fig. 3(a) and Fig. 3(b) that the numerical calculation matches very well with Euler buckling theory.

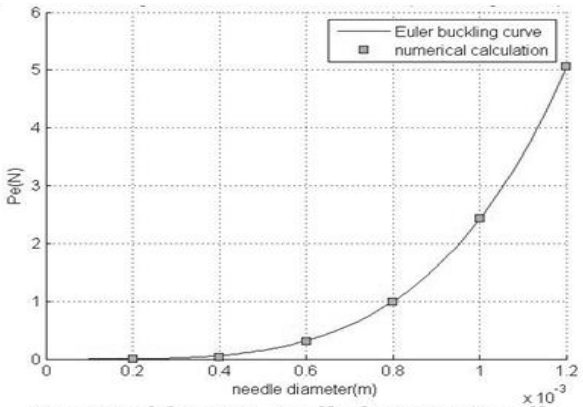

(a) critical force vs. needle diameter (needle length: 0.1 mm).

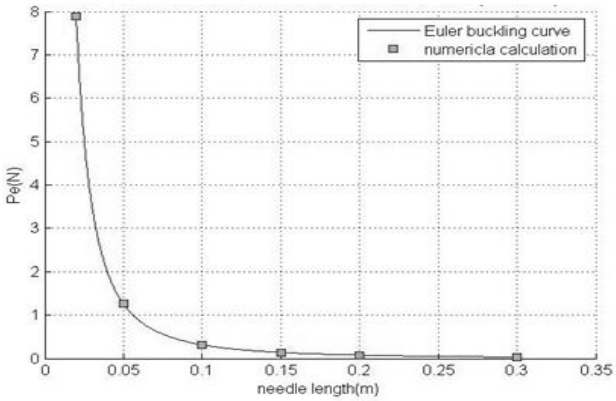

(b) critical force vs. needle length (d=0.6mm).

Fig. 3. Plots of buckling critical forces versus needle radius and length.

B. Needle Buckling in Homogeneous Tissue

Fig. 4(a) is the sketch of a buckling model in homogeneous tissue. The end of the column is fixed, and the other is free and applied with an axial load F. It is sustained by springs with stiffness μ. The buckling critical force is calculated with the following equation [2]:

$$P_e = \frac{\pi^2 EI}{4l^2} + \frac{\mu l^2}{\pi^2} \tag{2}$$

However, for a given tissue to be simulated, its Young's modulus is known, and its corresponding spring stiffness is unknown. In order to get the critical force by using Equation (2), the relationship between Young's modulus of tissue and

its spring constant needs to be obtained. As mentioned before, the Euler critical force can be well approximated by numerical solution. Replacing the theoretic critical force P_e with the numerical solution, $P_e^{'}$, the spring constant is derived as:

$$\mu \approx \frac{\pi^2 P_e^{'}}{l^2} - \frac{\pi^4 EI}{4l^4} \tag{3}$$

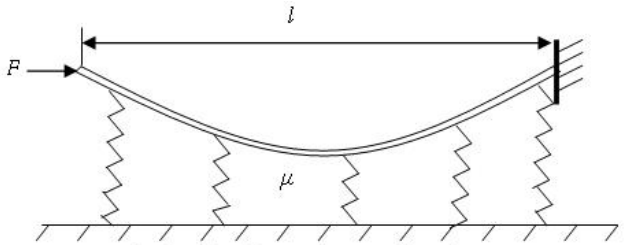

(a) sketch of buckling with spring foundations;

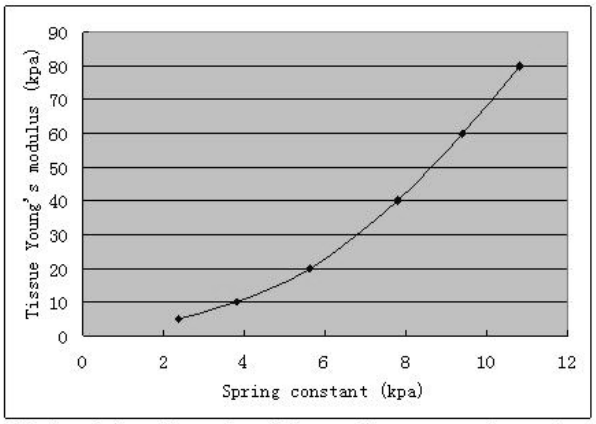

(b) plot of tissue Young's modulus and its corresponding spring constant;

Fig. 4. Needle buckling model in homogeneous tissue.

For a needle with a length of 50 *mm*, radius of 0.3 *mm*, and Young's modulus of 2×10^{11} *pa*, the curve of tissue Young's modulus and its corresponding spring stiffness is plotted as shown in Fig. 4(b) based on Equation (3). From this curve, the critical force can be calculated and used in the haptic rendering for various tissue's Young's modulus and needle insertion depths. In the numerical solution, the homogeneous tissue is simply modeled as a block with a volume of $10\times10\times50$ (mm^3), and the needle has a radius of 0.31 *mm* as shown in Fig. 5 (a) and (b). The tissue and the needle are assembled by constraining the needle in a hole in the block volume. The contact condition between the tissue and needle is set to a bonded type. Two faces of the tissue and one end of the needle are fixed as boundary conditions. Fig. 5(c) shows the deformations of needle and tissue after an axial load is applied. It can be seen from the figure that the deformations mainly take place near the needle free end.

C. *Needle Buckling in Multi-Layered Tissues*

Fig. 6(a) shows the model of needle buckling in two-layered tissues. From numerical calculation the needle buckling critical forces can be obtained in terms of different combinations of tissue elastic factors and their length proportions with regards to the overall length *l* of the needle. A sample set of data is given in Table 1. In this sample calculation, the needle length is 50 *mm*, radius is 0.3 *mm*, and the needle Young's modulus is 2×10^{11} *pa*. From the table, it can be seen that the tissue elastic factor near the free end of the needle plays a more important role in determination of the critical force. From rows 1, 3, and 5 of the table, as we can see that the length proportions change a lot, however, the critical forces have very little change. It might be explained as that the main deformations of tissue and needle occur near the free end of the needle. The deformations of tissue and needle in the other end are relatively small as shown in Fig. 5(c).

Using similar method three-layered tissues are modeled and analyzed as shown in Fig. 6(b) and Table 2. The difference between the data in row 1, 3, and 5 of Table 1 and that of row 1, and 3 in Table 2 is very small, though there is an extra layer tissue with large elastics in this model.

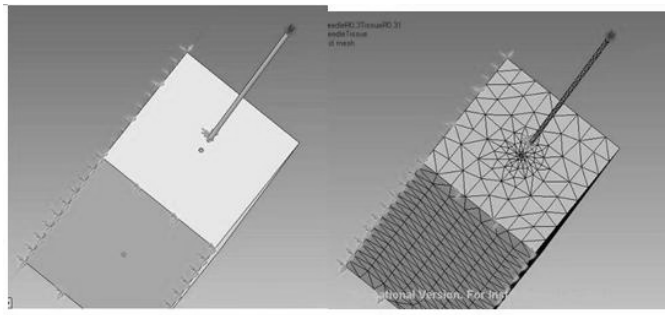

(a) solid model and its boundary conditions; (b) model mesh;

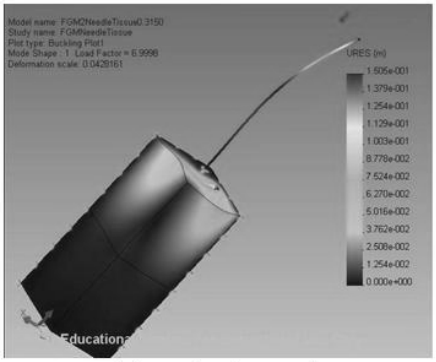

(c) analysis result;

Fig. 5. Needle and tissue simulation based on numerical calculation.

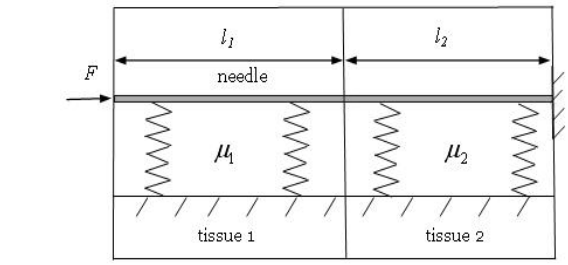

(a) Schematic of two-layered tissue model;

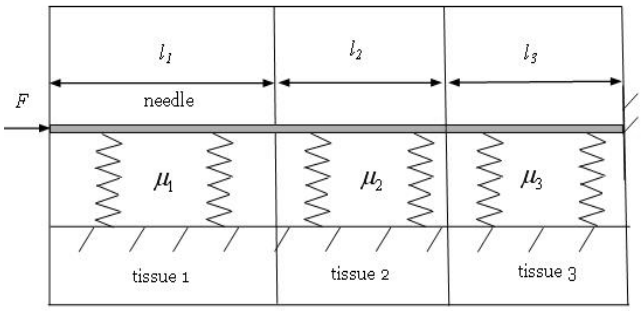

(b) Schematic of three-layered tissue model;

Fig. 6. Needle buckling model in multi-layered tissues.

Table 1. Buckling critical forces in a sample of two-layered tissue.

μ_1(pa)	μ_2(pa)	l_1/l	l_2/l	P_e(N)
5629.129	7792.546	0.5	0.5	7.000
7792.546	5629.129	0.5	0.5	9.001
5629.129	7792.546	0.25	0.75	6.994
7792.546	5629.129	0.25	0.75	8.659
5629.129	7792.546	0.75	0.25	6.909
7792.546	5629.129	0.75	0.25	9.058

Table 2. Buckling critical forces in a sample of three-layered tissue.

μ_1(pa)	μ_2(pa)	μ_3(pa)	l_1/l	l_2/l	l_3/l	P_e(N)
5629.129	7792.546	8915.707	0.2	0.4	0.4	7.179
8915.707	7792.546	5629.129	0.2	0.4	0.4	10.078
5629.129	7792.546	8915.707	0.25	0.25	0.5	7.172
8915.707	7792.546	5629.129	0.25	0.25	0.5	10.337

D. Large Deflection

Consider an elastic column of length l and bending rigidity EI in 2D as shown in Fig. 2. When the axial compressive force F is applied at both ends of the column, the deflection $w(x)$ takes place in the following form:

$$w(x) = a\sin(\frac{\pi x}{s}) = \frac{s}{\pi}\tan(\alpha)\sin(\frac{\pi x}{s}) \tag{4}$$

where a is the maximum deflection, x varies from 0 to s, s is the span of the beam and α is the slope angle at ends. α can be numerically calculated according to [2]:

$$\int_0^{\pi/2} \frac{dw}{\sqrt{1-\sin^2\frac{\alpha}{2}\sin^2 w}} = \frac{\pi}{2}\sqrt{\frac{F}{P_e}} \tag{5}$$

where P_e is the Euler buckling load (Equation 1), and F is the loading force applied to needle which will be explained in the next section. Using Equation (1), we can rewrite the above equation as:

$$\int_0^{\pi/2} \frac{dw}{\sqrt{1-\sin^2\frac{\alpha}{2}\sin^2 w}} = \frac{l}{2}\sqrt{\frac{F}{EI}} \tag{6}$$

III. FORCE MODELING

An energy-based method, similar to the way proposed in [4], is used to model the force, F_h, generated in the needle insertion process with following equation:

$$F_h = -F_t = -(\frac{\Delta U}{\Delta x} + \frac{2\pi J_c r \Delta l}{\Delta x}) \tag{7}$$

where r is the needle radius and Δl is the insertion depth increase, Δx is the tool displacement, ΔU is the change of elastic potential energy, J_c is fracture toughness.

The entire process of needle insertion can be reduced to two stages: deformation and penetration. If the exerted force on the tissue is smaller than the tissue rupture force, the tissue will only deform and won't be ruptured. Otherwise, deformation and penetration will be observed. In deformation stage, the work done by a needle is transferred into elastic energy U, stored in deformed tissue. The tissue recovers to initial states with the releasing of the elastic energy if the exerted force is removed. While in penetration stage, the work done by a needle equals to the summation of the elastic energy U and irreversible work spent on tissue piercing.

IV. AN EXPERIMENTAL CASE STUDY

Based on the above modeling methods for tissue deformation, flexible needle buckling and deflection, and force modeling, a flexible needle insertion simulator is developed as shown in Fig.8. The system is configured as shown in Table.3; and the simulation methods and parameters are listed in Table.4. In this simulator, a user can manipulate a virtual needle by means of the haptic stylus (Fig.9(a)). The needle parameters, e.g. radius and length can be selected by the user. If the needle tip touches the tissue, the tissue will deform and the user can feel feedback force through the haptic interface. If the user further pushes the needle, it may buckle and deflect as shown in Fig. 9(b). If the external force applied to the tissue is larger than its rupture force, then the needle will pierce into the tissue. And the needle deflection

will disappear (Fig. 9(c)). The feedback force will increase as the user further inserts the needle into the tissue. The buckling force is dynamically updated using Equation10 as the length of the needle outside the tissue decreases. If the driving force is larger than the buckling force, the second buckling will be observed as shown in Fig. 9(d). If the user selects a needle with short enough length or big enough radius, the needle buckling and deflection won't be observed during the insertion process.

The influence of needle parameters to insertion process is illustrated as shown in Fig.10. In the first experiment, the needle radius is set to 0.3 *mm*. As seen from Fig.10(a), when the needle length equals to 150 *mm*, the driving force increase almost linearly while the needle is inserted into the tissue before it penetrates the tissue. When the driving force is larger than the rupture force (1 *N*), the needle pierces into the tissue and the force decreases sharply. Then, the force increases as the needle is further inserted into the tissue. When the needle length is set to 200 *mm*, force fluctuates before tissue is penetrated. The force fluctuation is attributed to needle buckling. As the length is set to 300 *mm*, the needle buckling occurs with a smaller driving force. In the second experiment, the needle length is set to 200 *mm*. Similar trend as in Fig.10(a) is observed with the decrease of the needle radii as in Fig.10(b).

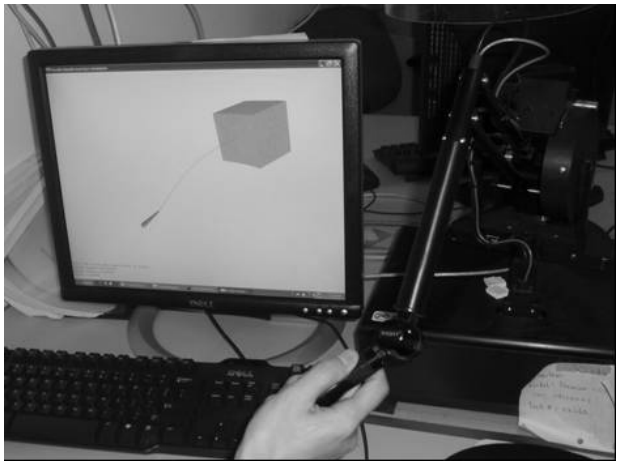

Fig. 8. System setup of the flexible needle insertion simulator based on a haptic interface.

Table 3. Simulation system setup.

computer	Dell® precision PWS670; a dual-processor Xeon (TM) 2.8 GHz with 1GB RAM; NVIDIA Quadro graphic card;
Operation system	Microsoft Windows XP
Haptic interface	Phantom® Premium 1.5/6-DOF device
Haptic rendering tool	OpenHaptics (SensAble®) API
Graphic rendering tool	OpenGL®

Table 4. Simulation data.

Tissue modeling method	co-rotational FEM
Material type	homogeneous
Yong's modulus	25 kpa
Poisson ratio	0.49
Needle model	Beam theory
Mesh subdivision	none

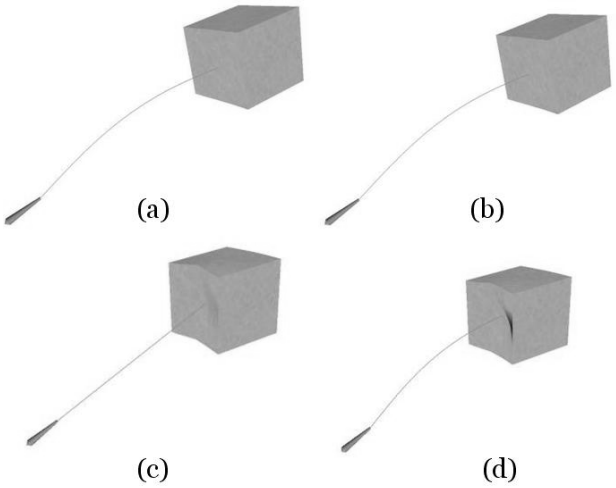

Fig. 9 Screen shots of the process of a needle insertion simulation.

V. CONCLUSIONS AND FUTRUE WORK

In this paper, a method on flexible needle insertion simulation is proposed. Needle buckling and deflection is modeled according to beam-columns theory and numerical calculations. A co-rotational FEM is used to model homogeneous tissue deformation, and a method based on mass-spring model is proposed for modeling deformation of layered tissue. A fracture mechanics approach is used to model the feedback force for haptic rendering. An experimental system is developed based on the modeling methods of tissue deformation, flexible needle buckling and deflection, haptic rendering. Through this system, a user can better understand the flexible needle insertion process.

Many aspects need to be further considered and improved. During the insertion process, the mesh topology modification is not taken into account since the needle radius is always smaller than 1mm. The technique of dynamic mesh subdivision is used in the simulation of needle insertion, e.g. [5]. However, it might increase the computation complex and induce system instability. Although needle buckling in

multi-layered tissues are studied in this paper using numerical calculations, an explicit equation needs to be derived in future work. The model of needle buckling in heterogeneous tissue needs further investigation too.

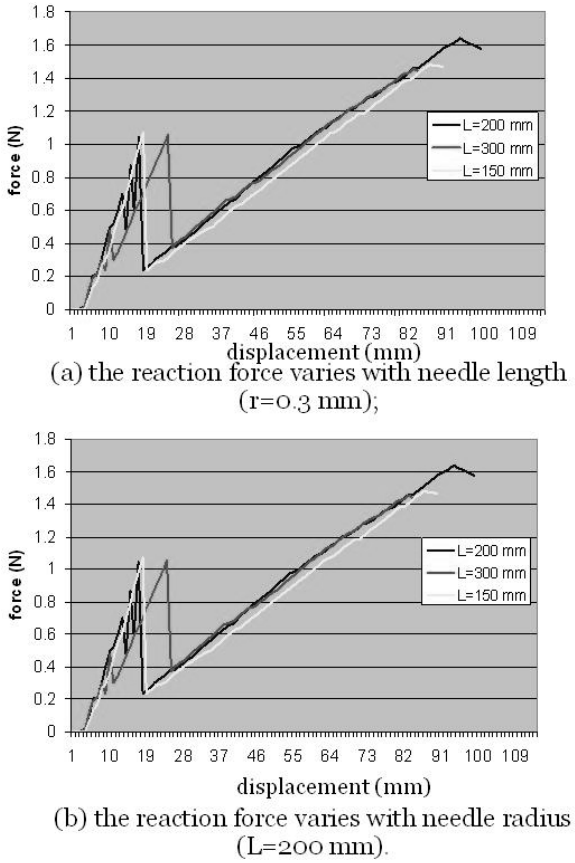

Fig. 10. Plots of reaction forces recorded from the haptic interface during needle insertion processes.

ACKNOWLEGEMENT

This research is supported by the grant HKU 710907E from Hong Kong Research Grants Council.

REFERENCES

[1] M. Müller, J. Dorsey, L. McMillan, R. Jagnow, and B. Cutler. Stable real-time deformations. Proceedings of ACM SIGGRAPH Symposium on Computer Animation, pages 49–54, 2002.

[2] Chen, W. F. and Atsuta, T., "Theory of Beam-Columns" Vol. 2, McGraw-Hill, 1977

[3] Atkins A. G., Mai Y-W., 1985. Elastic and plastic fracture: metals, polymers, ceramics, composites, biological materials, Chichester : Ellis Halsted Press.

[4] M. Mahvash and V. Hayward, "Haptic Rendering of Cutting, A Fracture Mechanics Approach," Haptics-e, The Electronic J. Haptics Research, vol. 2, no. 3, 2001.

[5] Simon P. DiMaio. Interactive Simulation of Needle Insertion Models. IEEE transactions on biomedical engineering, vol. 52, no. 7, p. 1167-1179, 2005.

[6] E. Gobbetti, M. Tuveri, G. Zanetti, and A. Zorcolo, "Catheter insertion simulation with co-registered direct volume rendering and haptic feedback," in Proc. Medicine Meets Virtual Reality 2000, Jan. 2000, pp. 96–98.

[7] T. Dang, T. M. Annaswamy, and M. A. Srinivasan, "Development and evaluation of an epidural injection simulator with force feedback for medical training," in Proc. Medicine Meets Virtual Reality, 2001, pp. 97–102.

[8] C. Simone and A. Okamura, "Modeling of needle insertion for robot assisted percutaneous therapy," in Proc. IEEE Int. Conf. Robotics and Automation, May 2002, pp. 2085–2091.

[9] http://www.solidworks.com/pages/products/cosmos/cosmosworks.html.

[10] http://www.vtk.org.

[11] F. L. Bookstein, Principal warps: Thin-plate splines and the decomposition of deformations, IEEE Trans. PAMI 11 (1989) 567.